

## THE DIFFUSE INTERSTELLAR CLOUD TOWARD HD 179406 (20 AQUILAE)

MARGARET MURRAY HANSON<sup>1</sup> AND THEODORE P. SNOW<sup>1</sup>Center for Astrophysics and Space Astronomy and Department of Astrophysical, Planetary, and Atmospheric Sciences,  
University of Colorado, Boulder CO 80309-0389

AND

JOHN H. BLACK

Steward Observatory, University of Arizona, Tucson, AZ 85721

Received 1991 August 23; accepted 1991 December 27

## ABSTRACT

We have completed an analysis of the diffuse interstellar cloud complex in front of HD 179406 (20 Aql). Along this sight line, multispectral absorption- and emission-line studies have uncovered at least three distinct velocity components due to individual clouds. A dominant velocity component is seen in both the absorption and emission-line data sets at  $3 \pm 1$  km s<sup>-1</sup>. We believe that the cloud associated with this velocity component is responsible for most of the atomic and all of the molecular gas in front of 20 Aql. Our chemical and physical analysis of the cloud combines the diagnostic tools of radio emission-line data with those of UV and optical absorption data. Using non-LTE models to synthesize the observed absorption profiles, we have determined the <sup>12</sup>CO and <sup>13</sup>CO column densities along this line of sight. The <sup>12</sup>CO/<sup>13</sup>CO abundance ratio was found to be  $50 \pm 15$ , similar to that found by Wannier et al. toward ζ Oph. We estimate that 40% of the hydrogen nuclei along this line of sight are in molecular form, using Lyα observations and chemical models that use carbon-based molecules to trace the molecular hydrogen content. The physical conditions of the cloud have been investigated using the ultraviolet [*A* <sup>1</sup>Π ← *X* <sup>1</sup>Σ] absorption lines of CO, the ultraviolet absorption lines from C I fine-structure states along with the optical [*B* <sup>2</sup>Σ ← *X* <sup>2</sup>Σ] absorption lines of CN. With these measurements we find that the dominant absorption cloud has a gas pressure similar to that found in the local diffuse molecular cloud in Ophiuchus (e.g., toward ζ Oph and χ Oph), with  $nT \approx 20,000$  cm<sup>-3</sup> K. However, not all the density indicators point toward the same gas temperature and density; we give arguments that most of the CN, C<sub>2</sub>, and <sup>13</sup>CO reside in a cooler, more dense region, while the dominant <sup>12</sup>CO seen lies in an extended warm neutral region, presumably surrounding the cool dense core.

*Subject headings:* ISM: abundances — ISM: clouds — ISM: molecules — stars: individual (20 Aquilae)

## 1. INTRODUCTION

In recent years chemical modes of diffuse interstellar clouds, guided by extensive absorption studies of various molecular and atomic species, have made great advances in determining physical conditions and chemistries (cf. van Dishoeck & Black 1986, 1988b). Owing to their large abundance and the accessibility of their spectra with present telescopes, carbon-based molecules such as C<sub>2</sub>, CH, CH<sup>+</sup>, CN, and CO are some of the most easily detected in diffuse clouds. This wealth of observational data has helped to make carbon chemistry the most thoroughly studied and best understood (e.g., Federman & Lambert 1988; Federman & Huntress 1989; van Dishoeck & Black 1989).

However, the abundances of several molecules and atomic species in diffuse clouds are still not easily explained. In an effort to assist in guidance of the models, and to understand better the range of relative abundances and varying physical conditions that exist in diffuse molecular clouds, we have completed a molecular and atomic abundance survey of the line of sight toward HD 179406. Also referred to as 20 Aquilae, this star is a B3 dwarf, with  $m_V = 5.34$ , a distance of  $\approx 200$  pc, and a moderate color excess of  $E(B - V) = 0.34$  (Savage et al. 1985;

Federman, Strom, & Good 1991). Along this sight line, absorption- and emission-line studies have uncovered at least three distinct velocity components due to individual clouds (Knapp & Jura 1976; Dickman et al. 1983; Federman et al. 1991). High-resolution ( $\lambda/\Delta\lambda = 200,000$ ) optical absorption spectra toward HD 179406 by Federman & Lambert (1992) show a single component in Ca I and CH<sup>+</sup> at  $+3-4$  km s<sup>-1</sup>, which corresponds to the position of the radio  $J = 1 \rightarrow 0$  CO line at 2.45 km s<sup>-1</sup> measured by Black & van Dishoeck (1992). We have combined our ultraviolet and optical data with the optical and radio data of others to perform this analysis. The absorption data have been obtained using the high-resolution spectrograph on the *International Ultraviolet Explorer* (IUE) and the coude spectrograph of the 3.6 m Canada-France-Hawaii Telescope (CFHT).

The plan of the paper is as follows. In § 2 we discuss the optical and ultraviolet observations made in this study. In § 3 we briefly describe the analysis leading to the atomic and molecular column density determinations. This section includes an atomic depletion study as well as a discussion of the modeling of the <sup>12</sup>CO and <sup>13</sup>CO absorption features. In § 4 we discuss our determination of the cloud physical conditions via calculation of  $\langle n_e \rangle$ , the mean electron density, and an analysis of the C I fine-structure states. A discussion that includes comparisons with other studies and combines our analysis into a single idea of the cloud's physical and chemical nature is found in § 5. A summary is found in § 6.

<sup>1</sup> Guest Observer with the *International Ultraviolet Explorer* satellite, which is sponsored and operated by the National Aeronautics and Space Administration, the Science Research Council of the United Kingdom, and the European Space Agency.

## 2. THE OBSERVATIONS

2.1. *The Ultraviolet Data*

Eight high-dispersion images from the *IUE* were used to create the final reduced spectrum. Four of the images (SWP 36939, SWP 36940, LWP 16282, LWP 16283) were part of our 12th episode *IUE* observing program. The other four spectra (SWP 8976, SWP 13865, LWR 7725, LWR 7726) were taken from the archives and reprocessed to the current pixel sampling rate. The images were interpolated to a common wavelength scale, cross-correlated, and co-added, to give average signal-to-noise levels of between 10 and 40 over the spectral range 1150–3200 Å. The archival data, which were taken over 8 years prior to our more recent spectra, required sufficiently large wavelength shifts relative to the calibrating reseau features that they were eliminated from the final co-added spectra. This was an important improvement to the spectra, since many interstellar features are lost due to blending with the numerous reseaux. We have also minimized the uncorrected pixel pattern noise by using these pixel-shifted co-adds.

2.2. *The Optical Data*

The observations were made with the CFHT on 1990 August 5–7. Data were recorded on the 1872 Reticon detector at the coudé focus in second order. This yielded a 2 pixel resolution of 0.07 Å, corresponding to an effective velocity resolution of 5 km s<sup>-1</sup>. The signal-to-noise ratio for targets as bright as HD 179406 should be controlled by photon statistics alone, but in the three wavelength ranges centered at 4300, 4230, and 3870 Å, the signal-to-noise values were actually determined to be, respectively, 500, 500, and 300 by measuring the standard deviation in the local line-free continuum regions. The three exposures in the region of the interstellar lines are shown in Figures 1a–1c.

## 3. DETERMINING COLUMN DENSITIES

Absorption strengths in a few lines were low enough to be unsaturated. In most cases, however, the absorption lines were saturated and a curve-of-growth method (Spitzer 1978) had to be used. For a few ions, such as Si II, Fe II, and Mg II, there are a sufficient number of absorption lines, spread over a large

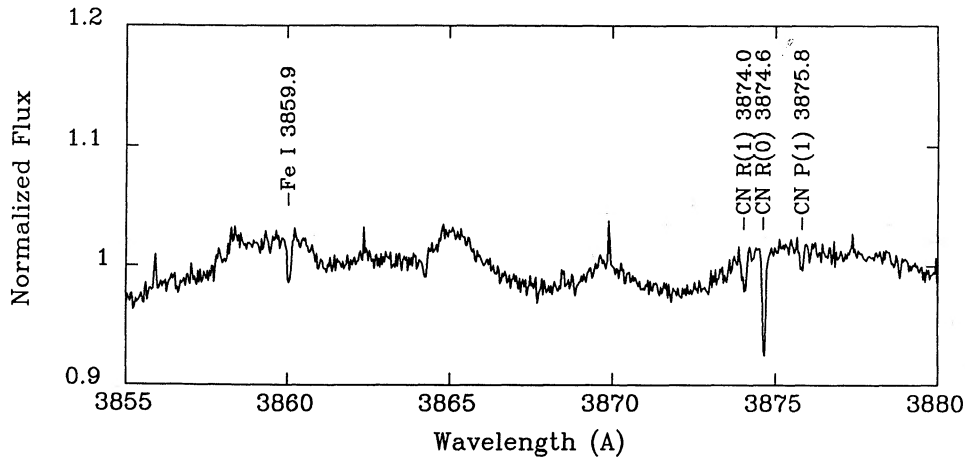


FIG. 1a

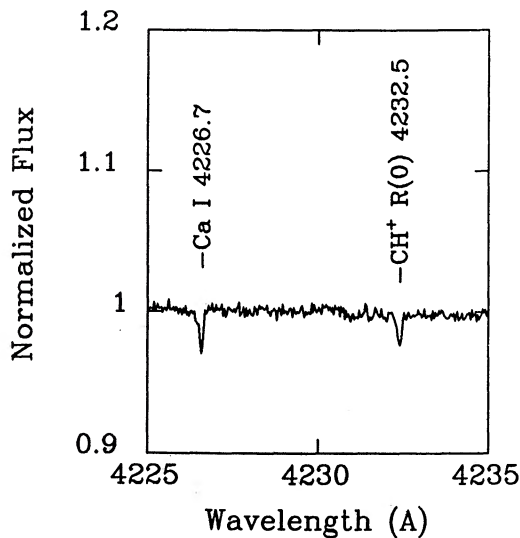


FIG. 1b

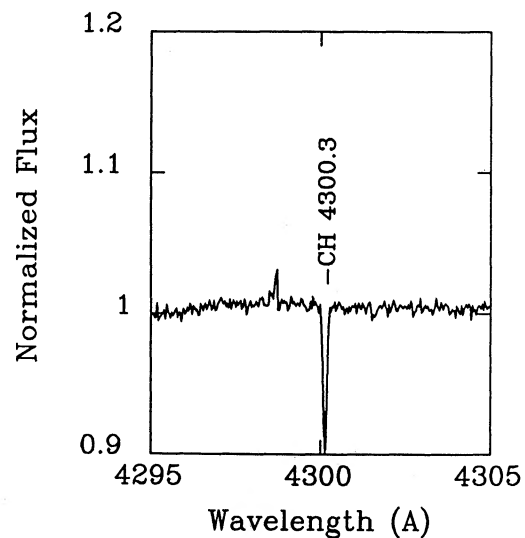


FIG. 1c

FIG. 1.—CFHT data, with flux normalized to unity

TABLE 1  
OBSERVED C I UV LINES

| Multiplet | Wavelength<br>(Å) | ( $J_r - J_u$ ) | $f$    | $W_\lambda$<br>(mÅ) |             |
|-----------|-------------------|-----------------|--------|---------------------|-------------|
| 7.01      | 1276.48           | 10-1            | 0.0045 | $20 \pm 5$          |             |
|           | 1276.75           | (1-1)           | 0.0029 | $11 \pm 5$          |             |
| 7         | 1277.25           | (0-1)           | 0.0740 | $120 \pm 10$        |             |
|           | 1277.28           | (1-2)           |        |                     |             |
|           | 1277.51           | (1-1)           | 0.0580 |                     |             |
|           | 1277.55           | (2-3)           |        |                     |             |
|           | 1277.72           | (2-2)           | 0.0160 |                     | $25 \pm 5$  |
|           | 1277.95           | (2-1)           | 0.0009 |                     | $7 \pm 5$   |
| 6         | 1279.06           | (1-2)           | 0.0018 | $23 \pm 5$          |             |
|           | 1279.23           | (2-3)           | 0.0049 | $12 \pm 5$          |             |
|           | 1279.50           | (2-2)           | 0.0007 | $5 \pm 4$           |             |
| 5         | 1279.89           | (1-2)           | 0.0136 | $30 \pm 5$          |             |
|           | 1280.10           | (0-1)           | 0.0241 | $45 \pm 5$          |             |
|           | 1280.34           | (2-2)           | 0.0146 | $10 \pm 5$          |             |
|           | 1280.40           | (1-1)           | 0.0044 | $28 \pm 8$          |             |
|           | 1280.60           | (1-0)           | 0.0068 | $25 \pm 5$          |             |
|           | 1280.85           | (2-1)           | 0.0050 | $20 \pm 5$          |             |
| 4         | 1328.83           | (0-1)           | 0.0640 | $43 \pm 6$          |             |
|           | 1329.09           | (1-0)           | 0.0625 | $70 \pm 10$         |             |
|           | 1329.10           | (1-2)           |        |                     |             |
|           | 1329.12           | (1-1)           |        |                     |             |
|           | 1329.58           | (2-2)           | 0.0620 |                     |             |
|           | 1329.60           | (2-1)           |        |                     |             |
| 3         | 1560.31           | (0-1)           | 0.0822 |                     | $80 \pm 10$ |
|           | 1560.68           | (1-2)           | 0.0740 | $75 \pm 5$          |             |
|           | 1560.70           | (1-1)           |        |                     |             |
|           | 1561.34           | (2-2)           | 0.0120 |                     |             |
|           | 1561.37           | (2-1)           |        |                     |             |
|           | 1561.44           | (2-3)           | 0.0600 |                     | $45 \pm 5$  |
| 2         | 1656.27           | (1-2)           | 0.0590 |                     | $60 \pm 8$  |
|           | 1656.93           | (0-1)           | 0.1420 | $145 \pm 20$        |             |
|           | 1657.01           | (2-2)           | 0.1000 |                     |             |
|           | 1657.38           | (1-1)           | 0.0370 | $52 \pm 8$          |             |
|           | 1657.91           | (1-0)           | 0.0480 | $40 \pm 5$          |             |
|           | 1658.12           | (2-1)           | 0.0360 | $25 \pm 5$          |             |

enough range in oscillator strength to provide a suitable choice for the Doppler  $b$  parameter. For the other ions, a suitable  $b$  was chosen based on the few data points available and a range consistent with the other elements. The  $b$ -values determined from Mg I and C I ( $J'' = 0$ ) were used to constrain the remaining neutral species. A listing of the C I lines with their identifications, oscillator strengths, and equivalent width measurements is given in Table 1. The remaining UV and optical atomic absorption lines detected are listed in Table 2. Atomic oscillator strengths were taken from Morton, York, & Jenkins (1988) or Morton (1991), except for the following: Si II from Luo, Pradhan, & Shull (1988); N I from Goldbach et al. (1986); Cl I from Clyne & Nip (1977); and C I from Nussbaumer & Storey (1984) and Goldbach & Nollez (1987). The molecular oscillator strengths for CN, CH<sup>+</sup>, and CH were taken from van Dishoeck & Black (1986) and Black & van Dishoeck (1988). The oscillator strengths for CO were calculated by one of us (J. H. B.), and are listed in Table 5.

The integration errors on the equivalent width determination, induced by statistical pixel-to-pixel signal fluctuations, were calculated using the procedure outlined by Jenkins et al. (1973). A second source of error, the continuum error, was determined by dividing the  $1 \sigma$  error of the continuum fit by the root number of independent pixels covering the feature. The *IUE* spectra are also plotted with other errors, such as the

TABLE 2  
OBSERVED ABSORPTION DATA

| Species | Wavelength<br>(Å) | $f$    | $W_\lambda$<br>(mÅ)      |
|---------|-------------------|--------|--------------------------|
| H I     | 1215.67           | 0.4162 | $(26 \pm 5) \times 10^3$ |
| C II    | 1334.53           | 0.1180 | $300 \pm 50$             |
| C II*   | 1335.71           | 0.1060 | $180 \pm 30$             |
| N I     | 1199.55           | 0.1330 | $170 \pm 30$             |
|         | 1200.22           | 0.0885 | $130 \pm 30$             |
|         | 1200.71           | 0.0442 | $100 \pm 30$             |
|         | 1302.17           | 0.0486 | $250 \pm 20$             |
| O I     | 1827.93           | 0.0230 | $25 \pm 8$               |
| Mg I    | 2025.82           | 0.1120 | $50 \pm 10$              |
|         | 2852.13           | 1.8100 | $170 \pm 15$             |
| Mg II   | 1239.93           | 0.0003 | $25 \pm 10$              |
|         | 1240.40           | 0.0001 | $20 \pm 10$              |
|         | 2795.53           | 0.5920 | $380 \pm 40$             |
|         | 2802.70           | 0.2950 | $340 \pm 40$             |
| Al II   | 1670.79           | 1.8800 | $160 \pm 10$             |
| Si I    | 1845.52           | 0.2290 | $13 \pm 6$               |
| Si II   | 1190.42           | 0.2913 | $130 \pm 30$             |
|         | 1193.29           | 0.5797 | $200 \pm 40$             |
|         | 1260.42           | 1.1467 | $200 \pm 50$             |
|         | 1304.37           | 0.1011 | $135 \pm 8$              |
|         | 1526.71           | 0.1165 | $155 \pm 8$              |
|         | 1808.01           | 0.0041 | $60 \pm 5$               |
| P II    | 1301.87           | 0.0170 | $20 \pm 10$              |
|         | 1532.51           | 0.0100 | $14 \pm 10$              |
| S I     | 1295.65           | 0.1080 | $20 \pm 10$              |
|         | 1425.03           | 0.1810 | $20 \pm 8$               |
| S II    | 1473.99           | 0.0782 | $15 \pm 10$              |
|         | 1807.31           | 0.1120 | $35 \pm 10$              |
|         | 1250.59           | 0.0054 | $85 \pm 10$              |
|         | 1253.81           | 0.0107 | $100 \pm 10$             |
|         | 1259.52           | 0.0159 | $95 \pm 10$              |
| Cl I    | 1188.77           | 0.0881 | $55 \pm 20$              |
|         | 1347.24           | 0.1120 | $45 \pm 5$               |
| Ca I    | 4226.73           | 1.7534 | $4.0 \pm 0.2$            |
| Cr II   | 2055.59           | 0.1670 | $13 \pm 8$               |
|         | 2061.54           | 0.1210 | $22 \pm 10$              |
|         | 2065.50           | 0.0798 | $< 8$                    |
| Mn II   | 2576.11           | 0.2880 | $105 \pm 10$             |
|         | 2593.73           | 0.2230 | $100 \pm 20$             |
| Fe I    | 2605.69           | 0.1580 | $95 \pm 20$              |
|         | 2483.27           | 0.5570 | $70 \pm 30$              |
|         | 2522.85           | 0.2790 | $15 \pm 10$              |
|         | 2719.03           | 0.1190 | $< 10$                   |
|         | 3859.91           | 0.0216 | $4.8 \pm 0.5$            |
| Fe II   | 1608.45           | 0.0620 | $85 \pm 10$              |
|         | 2343.49           | 0.1080 | $190 \pm 20$             |
|         | 2373.73           | 0.0393 | $140 \pm 15$             |
|         | 2382.03           | 0.3280 | $265 \pm 20$             |
|         | 2585.88           | 0.0570 | $220 \pm 20$             |
|         | 2599.39           | 0.2030 | $255 \pm 20$             |
| Ni II   | 1317.22           | 0.1210 | $15 \pm 10$              |
|         | 1741.55           | 0.0679 | $20 \pm 10$              |
| Cu II   | 1358.76           | 0.1196 | $< 10$                   |
| Zn II   | 2025.51           | 0.4120 | $85 \pm 10$              |
|         | 2062.01           | 0.2020 | $60 \pm 10$              |

calibrations of the zero flux level and flux errors due to scattered light. Several lines, such as H I  $\lambda 1216$ , C II  $\lambda 1334$ , Al II  $\lambda 1670$ , Fe II  $\lambda 2382$ , and Mg II  $\lambda 2796$ , should be completely saturated near their line centers and fall to zero flux, provided that the line center is spectrally resolved. However, a few percent error of the local continuum would not dominate over the continuum placement error if the local signal-to-noise ratio was less than 40, as is the case for our *IUE* data. For this reason, the final error in the total equivalent width was derived from the quadrature sum of the integration error and the continuum placement error only.

In the ultraviolet, the only H I line available is the highly damped 1215.7 Å Ly $\alpha$  line. The column density of H I toward HD 179406 was determined to be  $(4 \pm 1) \times 10^{21} \text{ cm}^{-2}$  via profile fitting of the damping wings (Bohlin 1975), giving a ratio of  $N_{\text{H I}}/E(B-V) = 1.2 \times 10^{22} \text{ cm}^{-2} \text{ mag}^{-1}$ . This is a bit high when compared with the mean interstellar ratio of  $5.2^{+4.3}_{-2.4} \times 10^{21} \text{ cm}^{-2} \text{ mag}^{-1}$  derived by Shull & Van Steenberg (1985), but *not* when compared with the average ratio of  $N_{\text{H I}}/E(B-V)$  seen toward B3 stars, which are believed to have contributions from the stellar atmosphere. For this reason, we have estimated the H I column density to be  $1.7 \times 10^{21} \text{ cm}^{-2}$  using the observed value of  $E(B-V)$  toward the star and the average ratio of  $N_{\text{H I}}/E(B-V)$  given in Shull & Van Steenberg (1985).

A list of atomic column densities, best-fit  $b$ -values, and estimated elemental depletions is given in Table 3. The total column density of hydrogen nuclei toward HD 179406 listed here has been estimated both by using the H I contribution and by estimating the H<sub>2</sub> contribution. A correlation between CO and H<sub>2</sub> column densities (Federman et al. 1980) gives  $N(\text{H}_2) = 6.9 \times 10^{20} \text{ cm}^{-2}$ , and between CH and H<sub>2</sub> column densities (Danks, Federman, & Lambert 1984) yields  $N(\text{H}_2) = 6.2 \times 10^{20} \text{ cm}^{-2}$  for the column densities  $N(\text{CO})$  and  $N(\text{CH})$  determined below. The average value,  $N(\text{H}_2) = 6.55 \times 10^{20} \text{ cm}^{-2}$ , together with the column density of H I, gives a total column density of  $N(\text{H}) = 3.0 \times 10^{21} \text{ cm}^{-2}$  hydrogen nuclei. The average column density of hydrogen nuclei per magnitude of color excess found by Bohlin, Savage, & Drake (1978),  $(\text{H} + 2\text{H}_2)/E(B-V) = 5.8 \times 10^{21} \text{ cm}^{-2} \text{ mag}^{-1}$  is lower than the ratio found toward HD 179406,  $(\text{H} + 2\text{H}_2)/E(B-V) = 8.8 \times 10^{21} \text{ cm}^{-2} \text{ mag}^{-1}$ . This may indicate either that the column density of hydrogen nuclei is overestimated or that the dust-to-gas ratio is lower than average along this line of sight. With an estimate of the total hydrogen column density, logarithmic depletions were determined (Van Steenberg &

Shull 1988) and are shown in Table 3. The values for solar abundances were taken from Morton et al. (1988).

With the CFHT we detected the (0-0)  $R(0)$  line at 4232.54 Å, due to the CH<sup>+</sup> [ $A^1\Pi \leftarrow X^1\Sigma^+$ ] electronic transition ( $3.3 \pm 0.8 \text{ mÅ}$ ) and the more saturated 4300.31 Å (0-0) ( $R_{2e} + R_{2f}$ ) line of the CH [ $A^2\Delta \leftarrow X^2\Pi$ ] transition (equivalent width  $12.6 \pm 1.3 \text{ mÅ}$ ). By using the curves of growth of van Dishoeck & Black (1989), we have accounted for the unresolved  $e$  and  $f$  components of the CH transition. Its column density error in Table 7 was determined for a range in  $b$ -values from 0.5 to 1.5 km s<sup>-1</sup>, which is the same range to which our CO absorption data can be confidently limited.

We observed the [ $B^2\Sigma^+ - X^2\Sigma$ ] (0-0) CN transitions centered at 3874 Å. Three transitions were detected, corresponding to the  $R(0)$ ,  $R(1)$ , and  $P(1)$  lines. The CN molecule decays radiatively from its excited levels quickly and will maintain a population distribution in equilibrium with the 2.7 K background radiation field,  $T_{\text{bg}}$ , provided that the density is low (a few hundred cm<sup>-3</sup>). If the density is unknown, then the effect of rotational excitation beyond  $T_{\text{bg}}$  must be considered. Table 4 lists the column densities of the  $N = 0$  and the  $N = 1$  states as a function of  $b$ -value. From the best-fitting column density in each state the corresponding rotational excitation,  $T_{10}$ , was determined (Meyer & Jura 1985). The total column density of CN varied from  $4.76 \times 10^{12}$  for  $b = 0.5 \text{ km s}^{-1}$ , to  $3.79 \times 10^{12}$  for  $b = 1.5 \text{ km s}^{-1}$ . Figure 2 shows results of that fit for the inputs  $b$ -value = 1.0 km s<sup>-1</sup>,  $T_{10} = 3.01 \text{ K}$ . The residual (data minus fit plus a constant) plotted at the bottom of Figure 2 shows the fit to be satisfactory. However, equally satisfactory fits were found for Doppler values from  $b = 0.8$  to  $b = 1.4 \text{ km s}^{-1}$ . The signal-to-noise ratio of our data was not sufficient to determine a significant best  $\chi^2$  fit among the range of inputs listed in Table 4. Usually the value of  $b$  can only be confidently determined by the use of resolved millimeter-wave emission lines of such species as <sup>13</sup>CO that can be attributed to the same cloud responsible for the absorption (cf. Gredel, van Dishoeck, & Black 1991).

TABLE 3

ATOMIC COLUMN DENSITIES AND DEPLETIONS

| Species     | log $N$<br>(cm <sup>-2</sup> ) | $b^a$<br>(km s <sup>-1</sup> ) | Depletion<br>(dex) |
|-------------|--------------------------------|--------------------------------|--------------------|
| H .....     | 21.5 ± 0.5                     | D                              | ...                |
| C I .....   | 15.0 ± 0.2                     | 4                              | ...                |
| C II .....  | 17.9 ± 0.3                     | D                              | -0.15              |
| N I .....   | <17.4                          | D                              | <-0.06             |
| O I .....   | 17.8 ± 0.2                     | 6                              | -0.6               |
| Mg I .....  | 13.6 ± 0.2                     | 4                              | ...                |
| Mg II ..... | 15.7 ± 0.2                     | 6                              | -1.4               |
| Al II ..... | 14.2 ± 0.3                     | 6                              | -1.8               |
| Si I .....  | 12.3 ± 0.1                     | L                              | ...                |
| Si II ..... | 15.0 ± 0.2                     | 9                              | -2.1               |
| P II .....  | 13.9 ± 0.2                     | L                              | -1.2               |
| S I .....   | 13.1 ± 0.1                     | 3-4                            | ...                |
| S II .....  | 16.1 ± 0.3                     | 6                              | -0.7               |
| Cl I .....  | 13.9 ± 0.3                     | 4                              | -0.9               |
| Ca I .....  | 10.1 ± 0.1                     | L                              | ...                |
| Ca II ..... | 12.3 <sup>b</sup>              | 8                              | -3.6               |
| Cr II ..... | 12.5 ± 0.2                     | L                              | -2.7               |
| Mn II ..... | 13.3 ± 0.2                     | 5                              | -1.7               |
| Fe I .....  | 12.3 ± 0.1                     | L                              | ...                |
| Fe II ..... | 14.3 ± 0.3                     | 8                              | -2.7               |
| Ni II ..... | 12.6 ± 0.2                     | L                              | -3.2               |
| Cu II ..... | <12.7                          | L                              | <-1.1              |
| Zn II ..... | 13.1 ± 0.3                     | 6                              | -1.1               |

<sup>a</sup> D indicates damped lines; L indicates unsaturated lines.

<sup>b</sup> Column densities taken from Spitzer et al. 1950.

### 3.1. The CO Spectrum

The fourth positive system [ $A^1\Pi \leftarrow X^1\Sigma$ ] of <sup>12</sup>CO and <sup>13</sup>CO is the most prominent of carbon monoxide in the ultraviolet region of the IUE (1140-3200 Å). Unfortunately, the determination of the CO column density is greatly hindered by the lack of adequate resolution. In our case, the high-dispersion echelle spectrograph on the IUE has an average

TABLE 4

CN EXCITATION TEMPERATURES

| $b$ -VALUE<br>(km s <sup>-1</sup> ) | COLUMN DENSITY<br>( $\times 10^{-2}$ ) |         | $T_{10} \pm 0.3$<br>(K) |
|-------------------------------------|--|---------|-------------------------|
|                                     | $N = 0$                                | $N = 1$ |                         |
| 0.5 .....                           | 3.38                                   | 1.38    | 2.73                    |
| 0.6 .....                           | 3.06                                   | 1.33    | 2.82                    |
| 0.7 .....                           | 2.90                                   | 1.32    | 2.88                    |
| 0.8 .....                           | 2.74                                   | 1.32    | 2.97                    |
| 0.9 .....                           | 2.70                                   | 1.32    | 3.00                    |
| 1.0 .....                           | 2.68                                   | 1.32    | 3.01                    |
| 1.1 .....                           | 2.63                                   | 1.32    | 3.04                    |
| 1.2 .....                           | 2.60                                   | 1.32    | 3.06                    |
| 1.3 .....                           | 2.57                                   | 1.32    | 3.08                    |
| 1.4 .....                           | 2.53                                   | 1.32    | 3.11                    |
| 1.5 .....                           | 2.48                                   | 1.31    | 3.13                    |

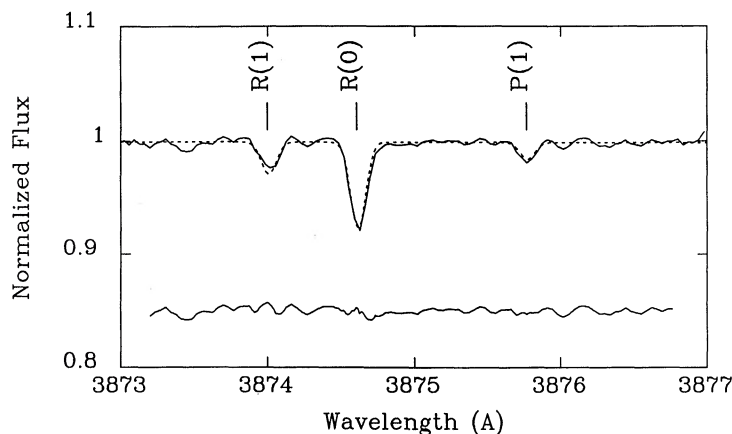


FIG. 2.—Synthesized profile plotted with the CN absorption spectra, with inputs rotational excitation,  $T_{10} = 3.01$ . Doppler  $b$ -value =  $1.0 \text{ km s}^{-1}$ , and  $N(\text{CN}) = 4.0 \times 10^{12}$ . Flux normalized to unity.

resolution of  $\lambda/\Delta\lambda \approx 13,000$ , which is insufficient to resolve the rotational structure within the electronic transitions. Further, as with the CN molecule, we must be concerned with the relative population of the ground-level rotational states. The gas density and temperature,  $n_{\text{gas}}$  and  $T_{\text{gas}}$ , must be known before a total column density can be determined. A curve-of-growth analysis is insufficient in determining all four variables, so profile fitting has been included to estimate the CO column density. Because we were unable to find a detailed table of the  $^{13}\text{CO}$   $[A-X]$  transitions in the literature, determination of the  $^{13}\text{CO}$  electronic transitions was carried out prior to modeling of our observed spectra. A description of these calculations, as well as an explanation of the Hönl-London factors used, has been included in the Appendix. The observed CO transitions and their equivalent width measurements are listed in Table 5.

### 3.1.1. Generating a Proper Curve of Growth for CO

Using *Copernicus* data, Wannier, Penzias, & Jenkins (1982) were able to use the very weak and unsaturated (11–0) and

(12–0)  $[A-X]$  lines toward  $\zeta$  Oph to determine their  $^{12}\text{CO}$  column density. With a known column density, they experimented with the Doppler  $b$ -value and LTE rotational temperatures,  $T_{\text{rot}}$ , to get best fits to their stronger lines. In the case of *IUE* data, only the strongest saturated lines can be routinely measured, and a curve of growth must be generated by calculating synthesized spectra, for various column densities,  $b$ -parameters, and ground-state rotational populations. Equivalent widths were determined by integrating the simulated spectra, and curves of growth empirically constructed by plotting the column density versus the resulting equivalent width. This method has been thoroughly discussed in Black & van Dishoeck (1988) and will be applied here.

Curves of growth were generated for various rotational populations corresponding to typical ranges in gas temperature (from 20 to 60 K) and density (from 200 to 1000  $\text{cm}^{-3}$ ). A family of curves was derived from a single rotational population over a range of Doppler  $b$ -values (generally from 0.5 to 3.0  $\text{km s}^{-1}$ ) and column densities (from  $N = 10^{12}$  to

TABLE 5  
OBSERVED CO LINES AND MOLECULAR CONSTANTS

| Wavelength <sup>a</sup><br>(Å) | Vibrational<br>Transition <sup>b</sup> | $f_{\nu\nu'}$<br>( $\times 10^{-3}$ ) | $W_{\lambda}$<br>(mÅ) | $\nu_0^c$<br>( $\text{cm}^{-1}$ ) | $B_{\nu}^c$<br>( $\text{cm}^{-1}$ ) | $D_{\nu}^c$<br>( $\times 10^{-6}$ )<br>( $\text{cm}^{-1}$ ) |
|--------------------------------|--|---------------------------------------|-----------------------|-----------------------------------|-------------------------------------|---|
| $^{12}\text{CO}$               |  |                                       |                       |                                   |                                     |   |
| 1544.451                       | (0–0)                                  | 15.63                                 | $150 \pm 10$          | 64744.72                          | 1.6002                              | 7.34  |
| 1509.750                       | (1–0)                                  | 34.39                                 | $115 \pm 5$           | 66232.98                          | 1.5786                              | 7.45  |
| 1477.568                       | (2–0)                                  | 41.27                                 | $130 \pm 5$           | 67675.66                          | 1.5571                              | 7.55  |
| 1447.355                       | (3–0)                                  | 36.06                                 | $120 \pm 5$           | 69088.48                          | 1.5347                              | 7.66  |
| 1419.046                       | (4–0)                                  | 25.80                                 | $110 \pm 6$           | 70466.86                          | 1.5115                              | 7.76  |
| 1392.525                       | (5–0)                                  | 16.10                                 | $90 \pm 8$            | 71809.02                          | 1.4876                              | 7.87  |
| 1367.622                       | (6–0)                                  | 9.104                                 | $75 \pm 10$           | 73116.69                          | 1.4633                              | 7.97  |
| 1344.183                       | (7–0)                                  | 4.791                                 | $63 \pm 6$            | 74391.75                          | 1.4389                              | 8.08  |
| 1322.147                       | (8–0)                                  | 2.390                                 | $45 \pm 10$           | 75631.73                          | 1.4146                              | 8.18  |
| $^{13}\text{CO}$               |  |                                       |                       |                                   |                                     |   |
| 1544.748                       | (0–0)                                  | 15.63                                 | <sup>d</sup>          | 64732.42                          | 1.530                               | 6.71  |
| 1510.507                       | (1–0)                                  | 34.39                                 | $95 \pm 6$            | 66199.92                          | 1.510                               | 6.80  |
| 1478.778                       | (2–0)                                  | 41.27                                 | $31 \pm 5$            | 67620.42                          | 1.490                               | 6.90  |
| 1449.142                       | (3–0)                                  | 36.06                                 | $23 \pm 6$            | 69003.41                          | 1.469                               | 6.99  |
| 1421.340                       | (4–0)                                  | 25.80                                 | $25 \pm 8$            | 70353.25                          | 1.447                               | 7.08  |
| 1395.220                       | (5–0)                                  | 16.10                                 | $12 \pm 6$            | 71670.43                          | 1.425                               | 7.18  |

<sup>a</sup> Corresponding to the R(0) rotational sublevel (Wannier et al. 1982).

<sup>b</sup> Electronic transition [ $A^1\Pi \leftarrow X^1\Sigma^+$ ].

<sup>c</sup> Corresponding to the upper ( $A^1\Pi$ ) electronic state.

<sup>d</sup> Blended and too weak to separate from  $^{12}\text{CO}$  (0–0) absorption line.

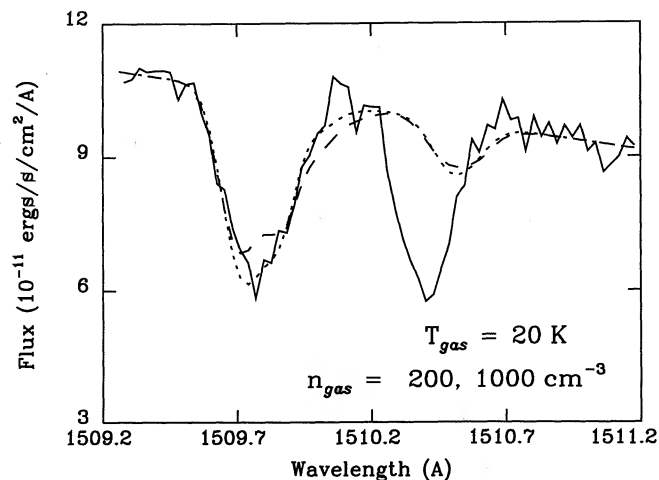


FIG. 3a

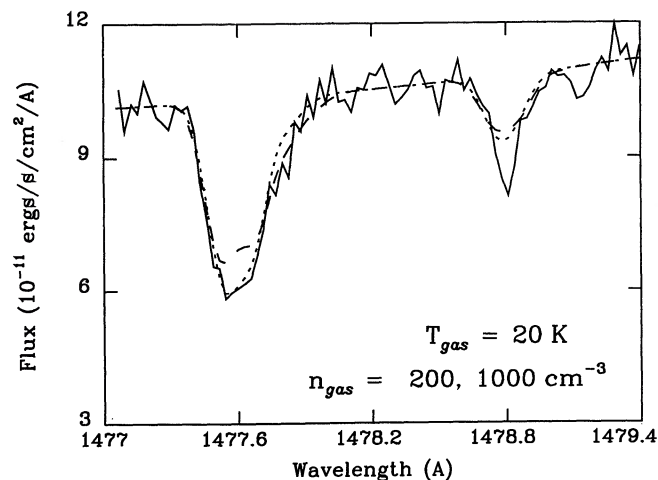


FIG. 3b

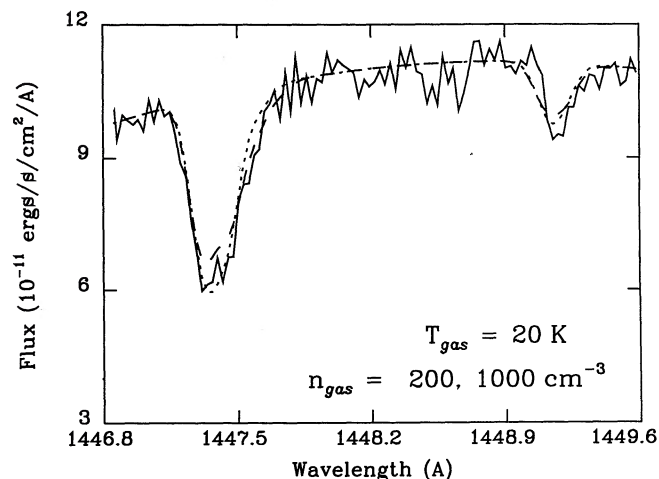


FIG. 3c

FIG. 3.—Synthesized profile plotted with the CO absorption spectra, with flux in units of  $10^{-11}$  ergs  $s^{-1}$   $cm^{-2}$   $\text{\AA}^{-1}$ . The gas temperature is 20 K;  $b = 1.4$  km  $s^{-1}$ ; the dotted line represents a gas density of  $200\text{ cm}^{-3}$ , and the dashed line a gas density of  $1000\text{ cm}^{-3}$ . (a) (1–0) transition. (b) (2–0) transition. (c) (3–0) transition.

$N = 10^{16}\text{ cm}^{-2}$ ). From each set of curves, a best-fit Doppler  $b$ -parameter and column density for that rotational population was determined through  $\chi^2$  minimization. Each set of parameters was then used to generate model absorption lines of the strongest CO bands [the (1–0), (2–0), (3–0), (4–0), and (5–0) electronic transitions], which were smoothed to the resolution of the *IUE* and then compared with our observed profiles. Each parameter set,  $N$ ,  $b$ ,  $T_{\text{gas}}$ , and  $n_{\text{gas}}$ , was selected because it predicted the observed equivalent widths of all the observed absorptions properly. The simulated spectra were used to determine which set of parameters reproduces the *shape* of the absorptions best.

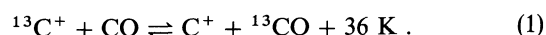
The simulated profiles for the  $^{12}\text{CO}$  and  $^{13}\text{CO}$  lines are shown in Figures 3, 4, and 5. The *IUE* data are shown plotted with the model results. The variation in the best-fit  $^{12}\text{CO}$  column density over these gas conditions was remarkably small, from  $2.3 \times 10^{15}$  to  $3.3 \times 10^{15}\text{ cm}^{-2}$ . However, the individual error in the curve-of-growth fit, as dictated by a 67% ( $1\sigma$ ) confidence of the  $\chi^2$  fit, increases the error. Our best-fit

estimate of the  $^{12}\text{CO}$  column density is  $3.0_{-1.5}^{+2.5} \times 10^{15}\text{ cm}^{-2}$ . The column density of  $^{13}\text{CO}$  was determined by first finding the best-fit  $^{12}\text{CO}$   $b$ -value for a certain  $J$  population and getting the best-fitting column density on these curves of growth. It was necessary to assume that the  $^{13}\text{CO}$  lines were described by the same  $J$  rotational populations and Doppler parameter as the  $^{12}\text{CO}$ , owing to the lack of constraints needed to determine these values independently. The best estimate of the  $^{13}\text{CO}$  column density is  $5.3_{-2}^{+3} \times 10^{13}\text{ cm}^{-2}$ , also based on the  $1\sigma$  confidence level from the  $\chi^2$  fits on the curve of growth. Satisfactory fits to our  $^{12}\text{CO}$  data were found for simulated profiles with  $T_{\text{gas}} = 20\text{ K}$  for a gas density of greater than  $500\text{ cm}^{-3}$ , for  $T_{\text{gas}} = 40\text{ K}$  for a gas density of  $200\text{--}500\text{ cm}^{-3}$ , and for  $T_{\text{gas}} = 60\text{ K}$  for a gas density of about  $200\text{ cm}^{-3}$ . Regardless of the gas temperature, a dominant  $^{12}\text{CO}$  gas density much greater than  $500\text{ cm}^{-3}$  is difficult to reconcile with the absorption profiles. The relatively low-quality fits to the  $^{13}\text{CO}$  data will be discussed in § 5. The most unusual feature, the (1–0)  $^{13}\text{CO}$  line at  $1510.5\text{ \AA}$ , cannot be due to  $^{13}\text{CO}$  alone (Wannier et al. 1982; Black 1980). It is thought to be an unidentified atomic or molecular feature coincident with the  $1510.5\text{ \AA}$   $^{13}\text{CO}$  line and was not used in the column density determination.

### 3.1.2. The $^{12}\text{CO}/^{13}\text{CO}$ Ratio

Models of the chemical evolution of the Galaxy predict that the  $^{12}\text{C}/^{13}\text{C}$  ratio should decrease as interstellar material becomes more processed as a consequence of stellar evolution. In an effort to understand the chemical evolution of the Galaxy, this ratio has been determined in many regions throughout the Galaxy. Radio CO measurements (Langer & Penzias 1990) give an average value of 30 within 5 kpc from the Galactic center, to about 70 at a radius of 12 kpc. Near the solar circle, they determined a value of about 57, while the solar value is about 90. This result is believed to support the notion of chemical evolution.

The fractionation of carbon isotopes in molecules such as CO is controlled through many competing processes, not just the relative isotopic carbon abundance. The abundances of isotopic molecules are controlled through temperature-dependent isotope exchange reactions such as (Watson, Anicich & Huntress 1976).



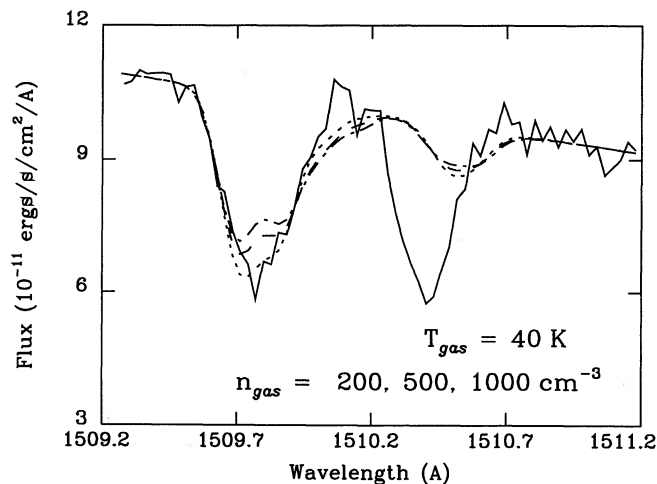


FIG. 4a

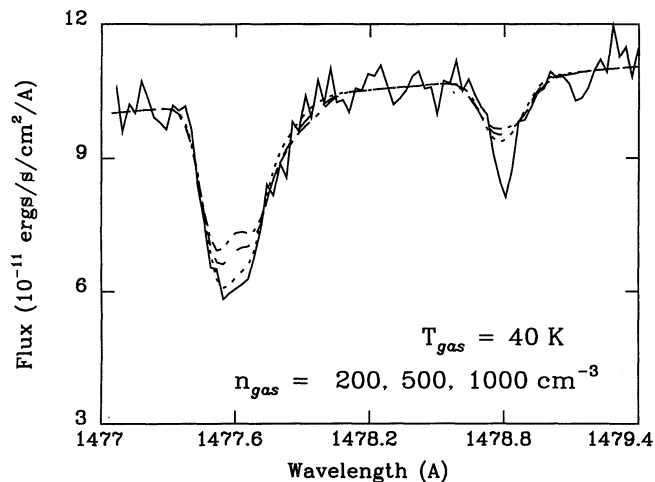


FIG. 4b

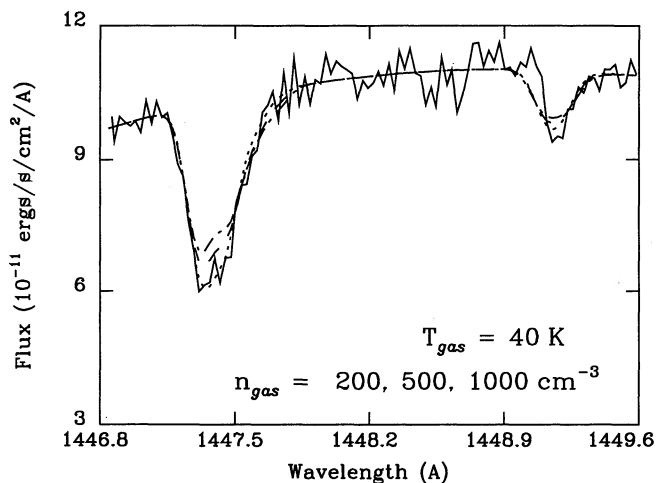


FIG. 4c

FIG. 4.—Synthesized profile plotted with the CO absorption spectra, with flux in units of  $10^{-11}$  ergs  $s^{-1}$   $cm^{-2}$   $\text{\AA}^{-1}$ . The gas temperature is 40 K;  $b = 1.2$  km  $s^{-1}$ ; the dotted line represents a gas density of  $200\text{ cm}^{-3}$ , the dashed line a gas density of  $500\text{ cm}^{-3}$ , and the dot-dash line a gas density of  $1000\text{ cm}^{-3}$ ; (a) (1–0) transition. (b) (2–0) transition. (c) (3–0) transition.

As the cloud cools to a gas temperature below 36 K, we would expect the  $^{12}\text{CO}/^{13}\text{CO}$  ratio to decrease. This reaction requires the existence of ionized carbon, which will become increasingly neutral as opacities increase.  $^{13}\text{CO}$  is also selectively destroyed from its larger photodissociation rate in diffuse clouds (Bally & Langer 1982). At an extinction typical of diffuse clouds,  $A_V^{\text{tot}} \approx 1.0$ , the photodissociation rate of  $^{13}\text{CO}$  is about 10 times that of  $^{12}\text{CO}$  (van Dishoeck & Black 1988a). We see, then, that the amount and *sense* of the fractionation varies with cloud conditions. The competing processes do tend to cancel each other over typical diffuse cloud conditions and sight lines; the difference between the  $^{12}\text{CO}/^{13}\text{CO}$  ratio and the  $^{12}\text{C}/^{13}\text{C}$  ratio should not be greater than 20%. But because of this uncertainty and because only one other study has been able to determine the ratio of  $^{12}\text{CO}/^{13}\text{CO}$  (Wannier et al. 1982), previous determinations of  $^{12}\text{C}/^{13}\text{C}$  have been based primarily on observations of carbon-based molecules such as CN and  $\text{CH}^+$  (cf. Hawkins, Jura, & Meyer 1985). Direct measurement of the  $^{12}\text{C}/^{13}\text{C}$  ratio is nearly impossible, owing to the extremely

small wavelength shift of atomic isotopes (see, e.g., Clark 1984).

In the present study of the sight line toward HD 179406, we find for the  $^{12}\text{CO}/^{13}\text{CO}$  ratio a value of  $50 \pm 15$ . This isotopic ratio was determined by fitting the two sets of equivalent widths on the same curve of growth. The error in the ratio is determined by the  $1\sigma$  confidence level of the minimum  $\chi^2$  for all points fitted on the same curve of growth, with the value of the ratio being the only free parameter. Thus, the determination of the ratio is independent of the model used for determining the  $^{12}\text{CO}$  column density. On the other hand, if either the rotational population or the  $b$ -parameter used for the  $^{13}\text{CO}$  model spectra is “colder” than that used for the  $^{12}\text{CO}$ , as the profiles seem to suggest, we will have underestimated saturation effects, and the  $^{13}\text{CO}$  column density will be higher than we have quoted. This would *decrease* our best estimate of the isotope ratio  $^{12}\text{CO}/^{13}\text{CO}$ . This point will be taken up again in § 6.

#### 4. PHYSICAL CONDITIONS OF THE DIFFUSE CLOUD

##### 4.1. CO and C I Fine-Structure Lines

As mentioned in § 3, it is necessary to know something about the physical conditions in the cloud in order to determine the column density of CO. Through profile fitting of the  $^{12}\text{CO}$  lines, we determined a  $T_{\text{gas}}$  of approximately  $40 \pm 20$  K, over a density range of from 200 to greater than  $500\text{ cm}^{-3}$  if the cloud is cold ( $< 40$  K), corresponding to an approximate  $nT = 20,000\text{ cm}^{-3}$  K. We can invoke further constraints on the local density and temperature of the gas with observations of the relative populations of the C I fine-structure levels. These follow from the equilibrium between collisional excitation by hydrogen atoms or molecules and spontaneous radiative decay of the upper levels (e.g., Jenkins & Shaya 1979; Jenkins, Jura, & Lowenstein 1983). By comparing the relative population of the C I fine-structure states (C I, 53%; C I\*, 33%; C I\*\*, 13%) with the figures of Jenkins & Shaya (1979), we found only weak support for the predicted values of interstellar pressure suggested by the CO data. The column densities of the C I fine-structure states are not well constrained because the lines are weak and only a few of each  $J$  state are separated enough from the other lines to be resolved by the IUE. A fairly wide range of pressures,  $nT \sim 3000\text{--}30,000\text{ cm}^{-3}$  K, in a general interstellar

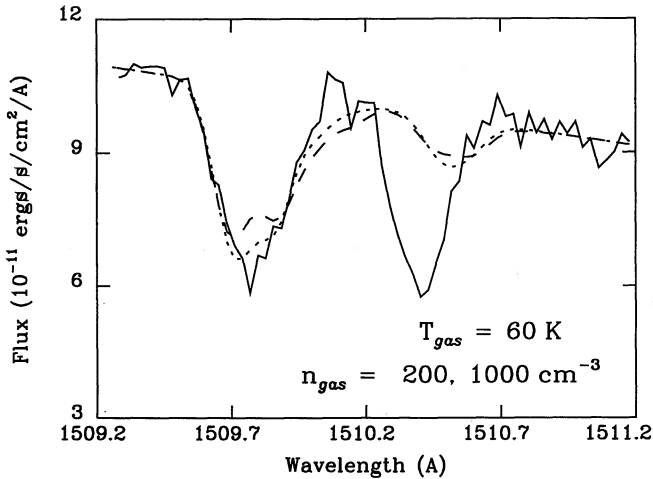


FIG. 5a

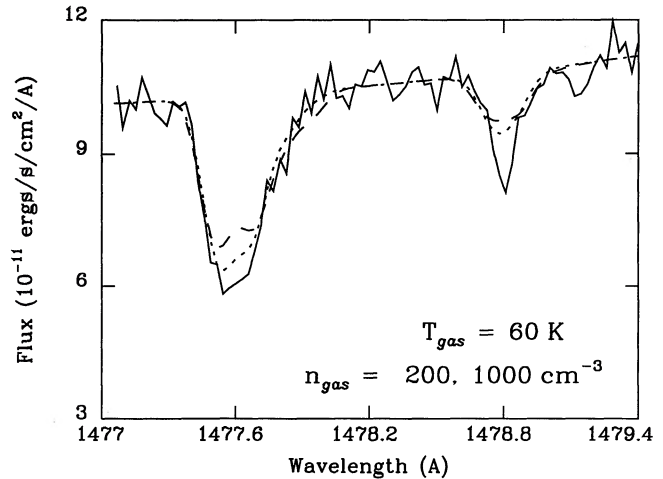


FIG. 5b

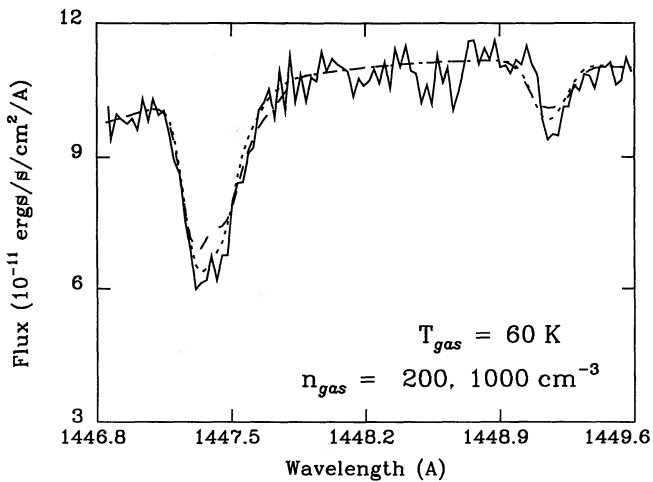


FIG. 5c

FIG. 5.—Synthesized profile plotted with the CO absorption spectra, with flux in units of  $10^{-11}$  ergs  $s^{-1}$   $cm^{-2}$   $\text{\AA}^{-1}$ . The gas temperature is 60 K;  $b = 1.0$  km  $s^{-1}$ ; the dotted line represents a gas density of  $200$   $cm^{-3}$ , and the dashed line a gas density of  $1000$   $cm^{-3}$ . (a) (1–0) transition. (b) (2–0) transition. (c) (3–0) transition.

radiation field (see Jenkins & Shaya 1979) would be consistent with the C I lines.

#### 4.2. Ionized and Neutral Abundances of Selected Atoms

The equation for photoionization equilibrium depends on the ratios of volume densities, but if one can assume that the species being compared occupy the same path length, the conversion to column density is valid. The electron density is given by

$$n_e = \frac{N_i}{N_{i+1}} \frac{\Gamma(I)}{\alpha(T)}, \quad (2)$$

where  $n_e$  is the volume density of electrons, and  $N_i$  and  $N_{i+1}$  are the column densities of the ionization stages  $i$  and  $i + 1$  for the same element. The photodissociation rate,  $\Gamma(I)$  ( $s^{-1}$ ), is a function of the radiation field intensity,  $I$ ;  $\alpha(T_{kin})$  ( $cm^3 s^{-1}$ ) is the radiative recombination rate coefficient, which is a function of kinetic temperature. Photoionization rates were taken from P equignot & Aldrovandi (1986), based on the ‘‘Standard UV’’

model of the radiation field intensity first proposed by Draine (1978) and later adapted by Roberge, Dalgarno & Flannery (1981) with a new functional form over the range 4–5.21 eV. Radiative recombination rate coefficients were determined from the work of Shull & Van Steenberg (1982) for two kinetic temperatures, 30 and 50 K. These values are given in Table 6.

If the neutrals and ions do not reside in the same cloud region, direct comparisons of the column densities are not valid and the values of  $n_e$  calculated cannot be directly interpreted as electron densities. However, Morton (1975) suggests that if the relative abundances of elements do not vary over the line of sight sampled, the mean  $n_e$ , referred to as  $\langle n_e \rangle$ , should be the same for all elements. Table 6 gives the results of the  $\langle n_e \rangle$  determined for six elements. The value of  $\langle n_e \rangle$  determined in this way ranges from  $\langle n_e \rangle \lesssim 0.1$   $cm^{-3}$  for the less depleted elements, C, Mg, and S, to  $\langle n_e \rangle \gtrsim 0.1$   $cm^{-3}$  for the more depleted elements, Si, Fe, and Ca.

#### 5. DISCUSSION

Up to this point, the technique of combining UV and optical absorption data with radio emission studies has been applied to only a few dark lines of sight (Januzzi et al. 1988; Crutcher 1985). The dense clouds along these sight lines have been named ‘‘translucent’’ molecular clouds (van Dishoeck & Black 1989) because they represent a transition between typical diffuse interstellar clouds and the very dark clouds commonly studied in the radio that are too opaque to be observed in absorption. In our study, we have combined the diagnostic

TABLE 6  
CALCULATION OF THE ELECTRON DENSITY

| Element  | Ionization Potential (eV) | $\Gamma(I)$ ( $s^{-2}$ ) | $\alpha(30$ K) ( $cm^3 s^{-1}$ ) | $\alpha(50$ K) ( $cm^3 s^{-1}$ ) | $\langle n_e \rangle$ ( $cm^{-3}$ ) |
|----------|---------------------------|--------------------------|----------------------------------|----------------------------------|-------------------------------------|
| C .....  | 11.26                     | 3.3(–10)                 | 1.76(–11)                        | 1.28(–11)                        | $0.01 \pm 0.005$                    |
| Mg ..... | 7.65                      | 7.1(–11)                 | 2.01(–11)                        | 1.30(–11)                        | $0.05 \pm 0.03$                     |
| Si ..... | 8.15                      | 3.1(–09)                 | 1.94(–11)                        | 1.42(–11)                        | $0.42 \pm 0.20$                     |
| S .....  | 10.36                     | 1.2(–09)                 | 1.60(–11)                        | 1.15(–11)                        | $0.11 \pm 0.06$                     |
| Ca ..... | 6.11                      | 4.3(–10)                 | 2.09(–11)                        | 1.32(–11)                        | $0.17 \pm 0.10$                     |
| Fe ..... | 7.87                      | 2.0(–10)                 | 2.51(–11)                        | 1.60(–11)                        | $0.12 \pm 0.07$                     |

NOTE.— $a(b)$  means  $a \times 10^b$ .

techniques offered by absorption and emission data to derive a more precise picture of the physical and chemical conditions of the clouds along the sight line to HD 179406. While the small color excess of HD 179406 would commonly categorize the sight line as being due to diffuse clouds, the absorptions seen appear to be dominated by a single cloud with high enough opacity and density to protect a large column density of molecules from photodestruction, as Table 7 illustrates. In other work along this same sight line, Black & van Dishoeck (1992) have observed the  $J = 1 \rightarrow 0$  line of  $^{12}\text{CO}$  and have measured a line strength of  $3.2 \text{ K km s}^{-1}$ , with a FWHM line width of  $2.71 \text{ km s}^{-1}$  (corresponding to a Doppler  $b$ -value of  $1.6 \text{ km s}^{-1}$ ) centered at  $2.5 \text{ km s}^{-1}$ . Federman & Lambert (1992) measured  $\text{CH}^+$  and  $\text{Ca I}$  with high resolution ( $\lambda/\Delta\lambda \approx 200,000$ ) and found a single component at  $3\text{--}4 \text{ km s}^{-1}$ .

Based on the above recent results, we tested the idea that the CO absorption and emission data were both sampling the same cloud. From our UV absorption analysis, we have determined the best-fit column density of CO to be  $3 \times 10^{15} \text{ cm}^{-2}$ , with a gas kinetic temperature of  $40 \text{ K}$ ,  $b = 1.2 \text{ km s}^{-1}$ , and gas density  $500 \text{ cm}^{-3}$ . Under these conditions, the brightness temperature integrated over the line should be  $3.3 \text{ K km s}^{-1}$ . Provided that the cloud fills the  $55''$  beam, the close match lends support to the idea that they are indeed seeing the same cloud. Measurement of the CO  $J = 2 \rightarrow 1$  line would confirm the results, as the intensity ratio of the  $J = 2 \rightarrow 1$  to the  $J = 1 \rightarrow 0$  line is very sensitive to density.

Nonetheless, we must acknowledge the inconsistency implied by the poor fits to the synthesized  $^{13}\text{CO}$  absorptions. The (2–0) and (3–0) transitions (Figs 3b and 3c), as well as some of the higher energy transitions not shown here, appear too deep and narrow to fit the synthesized features. The equivalent widths are well matched between the synthesized features and the observed data, but the poor fits to the line profiles may suggest that the  $b$ -value and/or gas pressure used are not correct for  $^{13}\text{CO}$  and that a colder rotational population or a smaller Doppler  $b$ -value than is determined from the  $^{12}\text{CO}$  analysis may be required. Gredel et al. (1991) explain that the abundance of the CO isotopes is controlled by a combination of the varying photodissociation rates and the effects of self-shielding. Their study of millimeter emission lines of CO isotopes showed that the  $b$ -value inferred from the radio  $^{13}\text{CO}$  emission was small,  $b \approx 1.0 \text{ km s}^{-1}$  or less. For the  $\text{C}^{18}\text{O}$ , an even smaller  $b$  was found. Because  $\text{C}^{18}\text{O}$  has a larger photodissociation rate than  $^{13}\text{CO}$  or  $^{12}\text{CO}$ , they predict that it would be less spatially extended. Such an isotopic segregation,

if it is also applied to  $^{13}\text{CO}$  and  $^{12}\text{CO}$ , would explain our CO absorption data. Gredel et al. also found that the CN toward all their sight lines had Doppler  $b$ -values in close agreement with the small  $b$ -value found from the  $^{13}\text{CO}$  emission data. This would suggest that the proper  $b$ -value to use for our CN data is less than the  $1.2 \text{ km s}^{-1}$  we found for the  $^{12}\text{CO}$ . If a Doppler  $b$ -value of  $1.2 \text{ km s}^{-1}$  or larger can be ruled out, then the density of the CN cloud is less than  $\approx 2000 \text{ cm}^{-3}$ . This is much larger than is suggested by our  $^{12}\text{CO}$  analysis, where we found difficulty in fitting densities above  $500 \text{ cm}^{-3}$ . Density determinations based on CN excitation are tricky (Black & van Dishoeck 1991). However, it is common practice to derive them from CN rotational states. They can be useful for obtaining a reasonable estimate of cloud density in the absence of better diagnostics.

Our data for the sight line toward HD 179406 are more easily interpreted if we apply a picture similar to that drawn in studies along other lines of sight; i.e., the cloud complex is described by varying physical and chemical conditions. Models of common sight lines, such as toward  $\zeta$  Oph, have used either a slowly varying cloud density and temperature (van Dishoeck & Black 1986) or two physically distinct components (Black & Dalgarno 1976, 1977; Viala, Roueff, & Abgrall 1988). Hard observational evidence of varying chemical conditions is only now becoming available. The recent high-resolution UV study of Joseph & Jenkins (1991) revealed three separate cloud components and two discrete H II regions along the line of sight to  $\pi$  Scorpii. Each of the cloud components appears as a distinct clump, one of which they identify solely as warm neutral medium (WNM) and the other two comprising cold clouds (CNM) with a small amount of WNM.

Because of the low ionization potential of Ca (6.1 eV), it can be assumed to remain photoionized through even the most dense regions of typical diffuse clouds. In a recent paper, Cardelli, Federman, & Smith (1991) find evidence for an anticorrelation between Ca I and CN. It has been known for some time that the CN molecule traces dense cloud regions. This is because its formation rate is strongly dependent on density (Federman, Danks, & Lambert 1984; Joseph et al. 1986). The Ca I atom was also thought to trace dense cloud regions. These arguments were based on simple ionization balance. Their findings suggest, however, that the Ca depletion is so strongly dependent on density, proportional to  $n^3$ , that the atom becomes depleted before significant recombination occurs. The large Ca depletion found toward HD 179406 in Table 3 indicates that the mean electron density determined in Table 6 is sampling the diffuse extended regions of the cloud, the WNM, only. In the WNM, the main source of electrons is through ionized C, assuming no depletion,  $\log(N_{\text{H}}/N_{\text{C}})_{\odot} = 3.44$ . Although low in abundance compared with carbon, Mg II, Si II, and Fe II can contribute some electrons, but they are probably slightly depleted in even the most diffuse regions (Joseph 1988). Using the  $\langle n_{\text{e}} \rangle$  value determined from Ca gives us a hydrogen space density in the WNM of

$$\langle n_{\text{H}} \rangle \approx \left( \frac{N_{\text{H}}}{N_{\text{C}}} \right)_{\odot} \langle n_{\text{e}} \rangle \approx 500 \text{ cm}^{-3}, \quad (3)$$

with an approximate factor of 2 error. The large depletion of Fe (and to a lesser extent Si and Mg) commonly seen in dense clouds would suggest that these elements may also be preferentially sampling the WNM. However, their larger ionization potentials of 7.9, 8.2, and 7.7 eV, respectively, may imply that they are becoming more neutral in darker cloud regions before

TABLE 7

COLUMN DENSITIES IMPORTANT IN CARBON CHEMISTRY MODELS

| Parameter or Species              | Observed           |
|-----------------------------------|--------------------|
| $n_{\text{H}}$ .....              | $500 \pm 300$      |
| $T$ .....                         | $40 \pm 20$        |
| $A_{\text{V}}^{\text{tot}}$ ..... | $0.95 \pm 0.1$     |
| H .....                           | $1.7 \pm 1(21)$    |
| $\text{H}_2$ .....                | $6.7(20)$          |
| $^{12}\text{CO}$ .....            | $3.0 \pm 2(15)$    |
| $^{13}\text{CO}$ .....            | $5.3 \pm 3(13)$    |
| CH .....                          | $2.0 \pm 0.5(13)$  |
| $\text{CH}^+$ .....               | $4 \pm 0.5(12)$    |
| CN .....                          | $4 \pm 2(12)$      |
| $\text{C}_2$ .....                | $8(13)^{\text{a}}$ |

<sup>a</sup>  $\text{C}_2$  data taken from Federman et al. 1991.

significant depletion has occurred. With the exception of Si, which shows a large error in  $\langle n_e \rangle$ , these indicators suggest a slightly smaller value for  $\langle n_e \rangle$ . This would lead to a value of  $\langle n_H \rangle < 500 \text{ cm}^{-3}$ . These results are consistent with the density determined for  $^{12}\text{CO}$ , which may be in error by a factor of 2 from our estimates. The remaining determinations of  $\langle n_e \rangle$  are not easily understood. The C-based value for  $\langle n_e \rangle$  is suspect, as both the C I and C II column densities are very difficult to determine. It should be reiterated, however, that it is presently unclear whether any single element will preferentially be sampling the darker portions of the cloud. Any value for  $\langle n_e \rangle$  determined for nondepleted elements would represent an average of the cloud electron density along the entire line of sight.

A final point to be made concerns the molecular data. The  $^{12}\text{CO}$  data, both UV absorption and radio emission, point toward a relatively large Doppler  $b$ -value and a low gas density. Other molecules,  $^{13}\text{CO}$  and, through indirect arguments (Gredel et al. 1992), CN, seem to suggest smaller  $b$ -values and possibly larger gas densities. A large fraction of the  $^{12}\text{CO}$  could reside in an extended warm, tenuous halo of WNM that also produces the dominant Ca I and  $\text{CH}^+$  seen in the high-resolution study of Federman & Lambert (1992), while only having trace amounts of  $^{13}\text{CO}$ , CN, and  $\text{C}_2$ . This would explain why our "pencil-beam" absorption analysis revealed results similar to those of the 55" beam emission analysis for  $^{12}\text{CO}$ . In the densest regions of the cloud, where conditions are described by higher elemental depletions, more dust, and therefore higher opacities, the larger spatial densities would give rise to the dominant absorption observed from the  $^{13}\text{CO}$ , CN, and  $\text{C}_2$  molecules. This would explain the chemical analysis toward HD 179406 of Federman et al. (1991). Their chemical models suggest a density of  $1500 \text{ cm}^{-3}$  toward HD 179406 based on the column densities of CN (the column density used was determined from the equivalent width quoted in Frisch 1972 and is more than a factor of 2 larger than our column density determination) and  $\text{C}_2$ . This is consistent with our analysis of the CN excitations in § 3. In order to understand the dark cloud component along this sight line, these

molecules should be utilized, since they are predominant in that region.

## 6. SUMMARY

While at least three cloud components have been identified in the optical and radio spectrum along this line of sight, one dominant absorption component, also traced in radio emission, appears to be the source of a relatively large column density of molecules. From the UV absorption data, we have determined the ratio of  $^{12}\text{CO}/^{13}\text{CO}$  to be  $50 \pm 15$  along this line of sight. Our analysis of the UV and optical spectra reveals conflicting evidence for the gas density in the dominant cloud component, leading us to envision that at least two gas phases are being seen in the same velocity component, one representing a warm neutral medium and a second tracing a cold neutral medium. The Ca and  $\text{CH}^+$  absorption spectra and  $^{12}\text{CO}$  emission spectra have been traced to the same velocity component, and comprise the extended WNM. The second phase, presumably surrounded by the halo gas, represents a region of increased gas density based on the profile analysis of CN,  $^{13}\text{CO}$ , and  $\text{C}_2$  which reside in this phase. This latter phase is only assumed to lie at the same velocity position as the first. We are without accurate velocity information for CN,  $^{13}\text{CO}$ , or  $\text{C}_2$  to prove this. Radio measurements of the  $^{13}\text{CO}$   $J = 1 \rightarrow 0$ , and the CN  $N = 1 \rightarrow 0$  at 113.491 GHz could determine the  $b$ -value and velocity of the second gas phase as well as confirm the excitation of CN.

M. M. H. is very grateful to S. R. Federman for comments that led to significant improvements in this paper and for communicating data prior to publication. We wish to thank C. L. Joseph, R. A. McCray, and D. E. Welty for useful discussions; P. W. Morris, J. M. Shull, and W. D. Vacca for critical reading of the manuscript; and J. C. Green and Q. Wang for help on error analysis. This work was made possible through a grant from NASA-IUE (contract NSG-5300) at the University of Colorado and the Colorado IUE Regional Data Analysis Center (contract NAS 5-28731). M. M. H. acknowledges support from the NASA Graduate Student Researchers Program.

## APPENDIX

The expression for the energy  $E_{v,J}$  of a rotating anharmonic oscillator with vibrational level  $v$  and in rotational level  $J$  can be written as a power series (Dunham 1932):

$$E_{v,J} = \sum_{ij} Y_{ij} (v + \frac{1}{2})^i J^j (J + 1)^j, \quad (4)$$

where  $Y_{ij}$  are the Dunham coefficients. These coefficients are approximated (see Herzberg 1950, p. 106, for exact definitions) by the more familiar band spectrum constants,  $Y_{10} \sim \omega_e$ ,  $Y_{20} \sim -\omega_e x_e$ ,  $Y_{01} \sim B_e$ ,  $Y_{02} \sim D_e$ , and the vibration-rotation crossterm  $Y_{11} \sim -\alpha_e$ . By using the ( $A^1\Pi$ ) coefficients of  $^{12}\text{CO}$  given in Tilford & Simmons (1972) and applying the appropriate isotope shift (see Herzberg 1950, p. 162) the coefficients for the ( $A^1\Pi$ ) state of  $^{13}\text{CO}$  were determined. From these, the rotational constants  $B_v$  and  $D_v$  were calculated for each vibrational state. The  $(v-0) R(0)$  transitions for  $^{13}\text{CO}$  given in Wannier et al. (1982) were used to determine empirically  $v_v$  (the energy difference between the upper vibrational state,  $v'$ , and the lower vibrational state,  $v'' = 0$ ). From these and our calculated rotational constants, the wavelengths for all the observable ( $\Delta J = 0, \pm 1$ ) electronic transitions were determined for the [ $A \leftarrow X$ ] transitions of  $^{13}\text{CO}$  using

$$v = v_v + B'_v J'(J' + 1) + D'_v J'^2 (J' + 1)^2 - [B''_0 J''(J'' + 1) + D''_0 J''^2 (J'' + 1)^2], \quad (5)$$

where the double prime refers to the lower state. The band constants used for the ( $X^1\Sigma$ ) lower state were  $B_0 = 1.92252$  and  $D_0 = -6.120 \times 10^{-6}$  for  $^{12}\text{CO}$  and  $B_0 = 1.83797$  and  $D_0 = -5.593 \times 10^{-6}$  for  $^{13}\text{CO}$  (from Guelachvili et al. 1983). The band constants used for the ( $A^1\Pi$ ) state are listed in Table 5. The accuracy of the calculated  $^{13}\text{CO}$  transitions was tested by using the same method to derive the corresponding  $^{12}\text{CO}$  transitions and then comparing them with the lists of Tilford & Simmons (1972). This method reproduced the published  $^{12}\text{CO}$  wavelengths to an accuracy of 0.01 Å.

Table 5 lists band oscillator strengths,  $f_{v'v''}$ , for the various vibrational-electronic transitions. The strength of any rotational line within that band is determined by multiplying the band oscillator strength by the appropriate Hönl-London factor. This relation is

$$f_{v'v''J'J''} = f_{v'v''} \frac{S_{J'J''}}{2J'' + 1} \frac{\lambda_{\text{band}}}{\lambda_{\text{line}}}, \quad (6)$$

where  $\lambda_{\text{band}}$  is the wavelength of the central band (the fictitious  $J' = 0 \leftarrow J'' = 0$  transition),  $\lambda_{\text{line}}$  is the wavelength of the transition of interest,  $(2J'' + 1)$  is the degeneracy factor, and  $S_{J'J''}$  is the Hönl-London factor. For the [ $A^1\Pi \leftarrow X^1\Sigma$ ] singlet transition of CO, the Hönl-London factors are given by

$$S_{J'J''} = \begin{cases} \text{R-branch} & (J' = J'' + 1): & \frac{J'' + 2}{2}, \\ \text{Q-branch} & (J' = J''): & \frac{2J'' + 1}{2}, \\ \text{P-branch} & (J' = J'' - 1): & \frac{J'' - 1}{2}, \end{cases}$$

for the three allowed transitions. A thorough discussion of the determination of the line strengths and Hönl-London factors of CN can be found in Federman et al. (1984).

## REFERENCES

- Bally, J., & Langer, W. D. 1982, *ApJ*, 255, 143  
 Black, J. H. 1980, in *IAU Symp 87, Interstellar Molecules* (Dordrecht: Reidel), 257  
 Black, J. H., & Dalgarno, A. 1976, *ApJ*, 203, 132  
 ———. 1977, *ApJS*, 34, 405  
 Black, J. H., & van Dishoeck, E. F. 1988, *ApJ*, 331, 986  
 ———. 1991, *ApJ*, 369, L9  
 ———. 1992, in preparation  
 Bohlin, R. C. 1975, *ApJ*, 200, 402  
 Bohlin, R. C., Savage, B. D., & Drake, J. F. 1978, *ApJ*, 224, 132  
 Cardelli, J. A., Federman, S. R., & Smith, V. V. 1991, *ApJ*, 381, L17  
 Clark, C. W. 1984, *ApJ*, 285, 322  
 Clyne, M. A., & Nip, W. S. 1977, *J. Chem. Soc. Faraday Trans. 2*, 73, 161  
 Crutcher, R. M. 1985, *ApJ*, 288, 604  
 Danks, A. C., Federman, S. R., & Lambert, D. L. 1984, *A&A*, 130, 62  
 Dickman, R. L., Somerville, W. B., Whittet, D. C. B., McNally, D., & Blades, J. C. 1983, *ApJS*, 53, 55  
 Draine, B. T. 1978, *ApJS*, 36, 595  
 Dunham, J. L. 1932, *Phys. Rev.*, 41, 721  
 Federman, S. R., Danks, A. C., & Lambert, D. L. 1984, *ApJ*, 287, 227  
 Federman, S. R., Glassgold, A. E., Jenkins, E. B., & Shaya, E. J. 1980, *ApJ*, 242, 545  
 Federman, S. R., & Huntress, W. Y. 1989, *ApJ*, 338, 140  
 Federman, S. R., & Lambert, D. L. 1988, *ApJ*, 328, 777  
 ———. 1992, private communication  
 Federman, S. R., Strom, C. J., & Good, J. C. 1991, *AJ*, 102, 1393  
 Frisch, P. 1972, *ApJ*, 173, 301  
 Goldbach, C., Martin, M., Nollez, G., Plomdeur, P., Zimmermann, J.-P., & Babic, D. 1986, *A&A*, 161, 47  
 Goldbach, C., & Nollez, G. 1987, *A&A*, 181, 203  
 Gredel, R., van Dishoeck, E. W., & Black, J. H. 1991, *A&A*, 251, 625  
 Guelachvili, G., de Villeneuve, D., Farrenq, R., Urban, W., & Verges, J. 1983, *J. Molec. Spectrosc.*, 98, 64  
 Hawkins, I., Jura, M., & Meyer, D. 1985, *ApJ*, 249, L131  
 Herzberg, G. 1950, *Molecular Spectra and Molecular Structure. I. Spectra of Diatomic Molecules* (New York: Van Nostrand)
- Januzzi, B. T., Black, J. H., Lada, C. J., & van Dishoeck, E. F. 1988, *ApJ*, 332, 995  
 Jenkins, E. B., Drake, J. F., Morton, D. C., Rogerson, J. B., Spitzer, L., & York, D. G. 1973, *ApJ*, 181, L122  
 Jenkins, E. B., Jura, M., & Loewenstein, M. 1983, *ApJ*, 270, 88  
 Jenkins, E. B., & Shaya, E. J. 1979, *ApJ*, 231, 55  
 Joseph, C. L. 1988, *ApJ*, 335, 157  
 Joseph, C. L., & Jenkins, E. B. 1991, *ApJ*, 368, 201  
 Joseph, C. L., Snow, T. P., Seab, C. G., & Crutcher, R. M. 1986, *ApJ*, 309, 771  
 Knapp, G., & Jura, M. 1976, *ApJ*, 209, 782  
 Langer, W. D., & Penzias, A. A. 1990, *ApJ*, 357, 477  
 Luo, D., Pradhan, A. K., & Shull, J. M. 1988, *ApJ*, 335, 498  
 Meyer, D. M., & Jura, M. 1985, *ApJ*, 297, 119  
 Morton, D. C. 1975, *ApJ*, 197, 85  
 ———. 1991, *ApJS*, 77, 119  
 Morton, D. C., York, D. G., & Jenkins, E. B. 1988, *ApJS*, 68, 449  
 Nussbaumer, H., & Storey, P. J. 1984, *A&A*, 140, 383  
 Peiquignot, D., & Aldrovandi, S. M. V. 1986, *A&A*, 161, 169  
 Roberge, W. J., Dalgarno, A., & Flannery, B. P. 1981, *ApJ*, 243, 817  
 Savage, B. D., Massa, D., Medde, U., & Wesselius, P. R. 1985, *ApJS*, 59, 397  
 Shull, J. M., & Van Steenberg, M. 1982, *ApJS*, 48, 95  
 ———. 1985, *ApJ*, 294, 599  
 Spitzer, L. 1978, *Physical Processes in the Interstellar Medium* (New York: Wiley-Interscience), 51  
 Spitzer, L., Epstein, I., & Hen, L. 1950, *Ann. Astrophys.*, 13, 147  
 Tilford, S. G., & Simmons, J. D. 1972, *J. Phys. Chem. Ref. Data*, 1, 147  
 van Dishoeck, E. F., & Black, J. H. 1986, *ApJS*, 62, 109  
 ———. 1988a, *ApJ*, 334, 771  
 ———. 1988b, in *Rate Coefficients in Astrochemistry*, ed. T. J. Millar & D. A. Williams (Dordrecht: Kluwer), 209  
 ———. 1989, *ApJ*, 340, 273  
 Van Steenberg, M. E., & Shull, J. M. 1988, *ApJ*, 330, 942  
 Viala, Y. P., Roueff, E., & Abgrall, H. 1988, *A&A*, 190, 215  
 Wannier, P. G., Penzias, A., & Jenkins, E. 1982, *ApJ*, 254, 100  
 Watson, W. D., Anicich, V. G., & Huntress, W. T., Jr. 1976, *ApJ*, 205, L165